Investigating the impacts of non-acyl peroxy nitrates on the global composition of the troposphere using a 3-D chemical transport model, STOCHEM-CRI

M. Anwar H. Khan[1], Barnaby Miles[1], Michael Jenkin[2], Dick Derwent[3], Carl J. Percival[4], Dudley E. Shallcross[1,5]*
[1]Biogeochemistry Research Centre, School of Chemistry, University of Bristol, Cantock's Close, Bristol BS8 1TS, UK
[2]Atmospheric Chemistry Services, Okehampton, Devon, EX20 4QB, UK
[3]rdscientific, Newbury, Berkshire, RG14 6LH, UK
[4]NASA Jet Propulsion Laboratory, California Institute of Technology, 4800 Oak Grove Dr, Pasadena, CA 91109, USA
[5]Department of Chemistry, University of the Western Cape, Robert Sobukwe Road, Bellville, 7375, South Africa.
*Author to whom correspondence should be sent
E-mail: d.e.shallcross@bristol.ac.uk
Phone: +44 (0) 117 928 7796

Abstract: Non-acyl peroxy nitrates, RO_2NO_2, act as a reservoir species for NO_x in the upper troposphere. The low thermal stability of these compounds means that they only become a significant sink of NO_x at the low temperatures observed in the upper troposphere. The chemical processes involved with the formation and degradation of methyl peroxy nitrate ($CH_3O_2NO_2$) and an additional forty-four RO_2NO_2 have been incorporated into the global 3-D chemical transport model, STOCHEM-CRI. The study investigates the effect of the addition of RO_2NO_2 chemistry on the budget of NO_x, which in turn impacts the ozone, hydroxyl radical (OH) and nitrate radical (NO_3) formation. This investigation found that the addition of $CH_3O_2NO_2$ led to an increase in the tropospheric burdens of NO_x (+3.0%), ozone (+2.0%), OH (+4.0%) and NO_3 (+8.8%). However, the other 44 RO_2NO_2 contribute a significant increment of tropospheric global burdens of NO_x (+4.4%), ozone (+3.4%), OH (+5.5%) and NO_3 (+11.1%) with largest mixing ratios of NO_x up to 25%, ozone up to 14%, OH up to 20% and NO_3 up to 50%. The increase in the global burden of oxidizing species like OH due to the addition of 44 other RO_2NO_2, led to a significant decrease in the lifetimes of greenhouse gases such as methane (~6%). The modelled mixing ratios of $CH_3O_2NO_2$ were in reasonable agreement with measurements, the only extensive dataset available.

KEYWORDS: Upper troposphere; chemical transport model; surface distribution; zonal distribution; global budget; oxidation cycle; atmospheric life-time; global fluxes; greenhouse gases;

1. Introduction

Peroxy nitrates, either acyl ($RC(O)O_2NO_2$) or non-acyl (RO_2NO_2), are the products formed from the series of reactions between volatile organic compounds (VOCs), hydrogen oxide radicals (HO_x), and nitrogen oxide radicals (NO_x).[1-2] Peroxy nitrates can be transported on regional scales, moving NO_x from source to receptor

regions and thus can affect the composition of the troposphere and climate by regulating the global budget of ozone and the Earth's oxidative capacity.[3-7] The thermal stability of RO_2NO_2 is weak at 300 K, leading to short lifetimes e.g. less than a second for non-acyl peroxy nitrates such as $CH_3O_2NO_2$ and ~30 minutes for acyl peroxy nitrates such as peroxyacetyl nitrate (PAN, $CH_3CO_3NO_2$, peroxyacetic nitric anhydride)[8-9] but increases at lower temperatures, more rapidly for acyl peroxy nitrates. Consequently, non-acyl peroxy nitrates (RO_2NO_2) may have little effect on the chemistry of the lower troposphere, but can have significant impact on the chemistry of the upper troposphere (as shown for $CH_3O_2NO_2$ by Murphy et al.[10]; Browne et al.[6]), whereas acyl-peroxy nitrates have long been known to play a role in boundary layer photochemical pollution.[11] Indeed, non-acyl peroxy nitrates can have significant mixing ratios in cold regions of the atmosphere (e.g. upper troposphere).[6,10,12-14] They are formed from the following association reactions (1):[15,16]

$$RO_2 + NO_2 + M \leftrightarrows RO_2NO_2 + M \qquad (1a, 1b)$$

The thermal decomposition in reaction (1b) is the main sink of RO_2NO_2 in the lower troposphere, and is strongly dependent on temperature.[13,17] Thus, their lifetimes increase with increasing altitude, resulting in a build up to significant concentrations in the upper troposphere. In the upper troposphere, photolysis and reaction with OH are expected to be the dominant loss processes.

The short lifetimes of RO_2NO_2 have several implications. The first being that at room temperature the lifetime of $CH_3O_2NO_2$ is shorter than 1 second, posing analytical challenges, particularly in aircraft sampling campaigns.[14] When air samples are collected, the warm interior of the aircraft results in substantial decomposition of RO_2NO_2 making measurements of the compound difficult, as well as giving positive interference to NO_2 measurements.[6,14] The second implication is that RO_2NO_2 species are only abundant at temperatures below about 240 K, so they can only act as a sink of NO_x and RO_2 and act as a temporary reservoir species for NO_x in the upper troposphere.[10] Even at these lower temperatures, they are important but short-lived sinks, existing for less than 24 hours due to thermal decomposition and reactions with OH radicals and photolysis.[18]

There are only two indirect and one direct set of measurement data available for the simplest RO_2NO_2 species: methyl peroxy nitrate ($CH_3O_2NO_2$). The sum of peroxy nitric acid (HO_2NO_2) and $CH_3O_2NO_2$ was estimated during the Tropospheric Ozone Production about the Spring Equinox (TOPSE) campaign by calculating the difference between total peroxy nitrate measurements and PANs.[10] This was estimated during the NASA Arctic Research of the Composition of the Troposphere from Aircraft and Satellites (ARCTAS) campaign by analyzing the temperature-dependent deviation of NO_2 observations from the photostationary state.[6] $CH_3O_2NO_2$ was observed directly during the Deep Convective Clouds and Chemistry (DC-3) and the studies of Emissions and Atmospheric Composition, Clouds, and Climate Coupling by Regional Surveys (SEAC^{4}RS) campaigns by direct detection of

$CH_3O_2NO_2$ using thermal-dissociation laser-induced fluorescence of NO_2 (TD-LIF).[14] The difficulty of direct observation of RO_2NO_2 in the atmosphere and the difficulty of isolation in the laboratory means that knowledge of the chemistry of RO_2NO_2 is limited. This has led to difficulties in comparison of modelled and measured data in past campaigns, where modelling of the total sums of HO_2NO_2 and $CH_3O_2NO_2$ concentrations became inaccurate at higher mixing ratios due to errors in the photochemistry of HO_2NO_2 and the thermal decomposition of $CH_3O_2NO_2$ in models.[10]

Modeling studies of the formation of $CH_3O_2NO_2$ and their impacts on the global composition of the atmosphere is sparse and very limited. Using the upper tropospheric measurement data from the Pacific Exploratory Mission in the Western Pacific Ocean (PEM-West B), Thompson et al.[19] simulated an average mixing ratio of 27 ppt $CH_3O_2NO_2$ at 10 km in the mid-latitudes (35-45^{o}N) using a 1-D tropospheric chemical model. Steady-state modeling by Cantrell et al.[20] found an average mixing ratio of 70 ppt $CH_3O_2NO_2$ at 40-60^{o}N and 27 ppt at 60-85^{o}N in the upper troposphere. The addition of $CH_3O_2NO_2$ chemistry to a global chemistry transport model, GEOS-Chem, showed measurable effects on the mixing ratios of NO_x, ozone, HNO_3, OH and HO_2.[6] There have been no attempts to explore the effects of the chemistry of other RO_2NO_2 species until now. In this study, we added the formation of other forty-four RO_2NO_2 species into the STOCHEM-CRI model, along with their loss processes (thermal decomposition, photolysis and reaction with OH), to investigate the impact of these compounds on the NO_x budget of the upper troposphere. This allowed the investigation of the impact of adding 44 other RO_2NO_2 on the budgets of tropospheric species that are influenced by the NO_x cycle, such as ozone, HO_x and NO_3.

2. Modelling

STOCHEM is a global tropospheric chemistry transport model, which adopts a Lagrangian approach. The Lagrangian approach uses 50,000 air parcels which, after each advection time step of 3 hours, are mapped to a 5° × 5° resolution grid with 9 vertical layers. These air parcels are advected by winds generated from the United Kingdom Meteorological office global circulation model (UM-GCM),[21] meaning that all trace gas species in the model are advected together, so the chemistry and transport processes can be uncoupled and the chemistry timesteps determined locally.[22] Archived meteorological data is generated at a resolution of 1.25° × 0.83° × 12 vertical levels. This includes winds but also pressure, temperature, humidity, cloud and precipitation; as well as tropopause heights and boundary-layer/surface parameters.[23-24] The meteorological parameterization of STOCHEM (e.g. vertical coordinate, advection scheme, boundary layer treatment, inter-parcel exchange and convective mixing) has been discussed in detail previously.[22,25] The convective transport scheme in STOCHEM has been evaluated against the observations of a short-lived tracer, ^{222}Rn.[24] The role of convection in determining the budget of odd hydrogen in the upper troposphere through the convection of isoprene and its carbonyl and hydroperoxide oxidation products has been reported elsewhere.[26]

The chemical mechanism used in STOCHEM is the 'Common Representative Intermediates mechanism version 2.2 and reduction 5' (CRI v2.2-R5). This is a reduced chemical scheme, which is required for atmospheric models due to computational limitations, and is achieved by reducing the complexity of the chemistry in the mechanism and by grouping emissions.[27-28] The current version, CRI v2.2-R5, was developed using the Master Chemical Mechanism version 3.3.1 (MCM 3.3.1), and a benchmark, reducing the number of species and reactions by 90%, and described in detail elsewhere.[27-30]

The additions of RO_2NO_2 in the CRI mechanism are performed by adding their formation from the reaction of peroxy radicals (RO_2) with nitrogen dioxide (NO_2) (reaction (1a) and their losses by thermal decomposition (reaction (1b), and by reaction with OH radical and by photolysis. The details of the species and their formation and loss reactions can be found in the Supplementary Information (Tables S1-S3). The rate coefficients for the formation and decomposition of $CH_3O_2NO_2$ and $C_2H_5O_2NO_2$, and generic rate coefficients applied to the formation and decomposition of other RO_2NO_2, are based on those recommended by Jenkin et al.[9]. There are no reported kinetic studies of the loss of RO_2NO_2 by reaction with OH, and the same rate coefficients currently applied to the corresponding alkyl nitrates ($RONO_2$) species in CRI were therefore used, i.e. it is assumed that the deactivating effects of $-ONO_2$ and $-OONO_2$ groups on OH reactivity are approximately the same, this being consistent with the approach applied in the Structure Activity Relationship (SAR) of Jenkin et al.[31]. The reaction products are simplified by assuming efficient release of NO_x (via NO_3) (see Table S2).

The rate of photolysis of a given species is calculated using the following integral

$$J_A = \int_0^\infty F(\lambda)\, \sigma_A(\lambda)\, \emptyset_A(\lambda)\, d(\lambda)$$

Where J_A is the photolysis rate of a given compound 'A', F (λ) is the spherically integrated actinic flux at a given wavelength, σ_A (λ) is the cross-section of compound A at a given wavelength, and $Ø_A$ (λ) is the quantum yield for dissociation of A at a given wavelength. The cross section and quantum yields are taken from the recommendations of either the Jet Propulsion Laboratory (JPL) kinetic evaluation reports[32,33] or the International Union of Pure and Applied Chemistry data evaluation (IUPAC; http://iupac.pole-ether.fr). According to IUPAC, the cross-sections of $CH_3O_2NO_2$ can be used as for HO_2NO_2 at wavelengths above 290 nm. The same photolysis parameters were therefore used for all RO_2NO_2. Based on the IUPAC recommendations for HO_2NO_2 at 248 nm, quantum yields of 0.59 and 0.41 were assigned to two photolysis product channels, forming $RO_2 + NO_2$ and $RO + NO_3$, respectively (see Table S3). The photolysis rates for each reaction in the model are calculated for each air parcel at a time resolution of one hour. These rates are then linearly interpolated with respect to time, yielding 5-minute resolution values, which are used in the chemical integration.

Emissions in the STOCHEM-CRI model are divided into three sub-sections: surface emissions, stratospheric sources and 3-D emissions. Surface emissions (e.g.

emissions from anthropogenic activity, biomass burning, oceans, soils etc.) are added using monthly 2-D source maps at a resolution of 5° × 5°.[34] This is large enough to give an average cell occupancy in the mid-latitudes (approximately two Lagrangian cells per grid square when within the boundary layer) but is too coarse to resolve individual pollution centres.[35] The 1998 'Precursor of Ozone and their effects on the Troposphere' (POET) inventory provided the total emissions for CO, NO_x and all non-methane VOCs.[36] The total emissions of CH_4 were obtained from the inverse model study by Mikaloff-Fletcher et al.[37] apart from ocean emissions, which were taken from Houweling et al.[38] The anthropogenic and biomass burning of benzene, toluene and o-xylene were taken from Henze et al.[39] The emission profiles of important RO_2NO_2 precursor compounds are shown in Supplementary Information Table S4.

The Lagrangian cells within the STOCHEM-CRI model are kept below 100 hPa so the air parcel exchange with the stratosphere is represented by the downward flux of ozone and HNO_3 into the top level of the model. The flux of ozone is calculated using 3-hourly vertical wind fields with monthly ozone fields from Li and Shine.[40] Based on the work of Murphy and Fahey[41], the HNO_3 flux is calculated as one thousandth of the ozone flux by mass of N.

Emission sources which inject species directly into the troposphere (e.g. lightning and aircraft emissions) are 3-D emissions. The data for lightning emissions are taken from Price and Rind[42] and are scaled so that the total global emission of NO_x from lightning is 5 Tg yr^{-1}. The total number of lightning flashes are calculated using the cloud heights, with different formulae being used for continental and maritime clouds. The relative amounts of cloud-ground and cloud-cloud flashes are calculated using the formula from Price et al.[43] NO_x production is calculated from the number of flashes and distributed vertically by using profiles from Pickering et al.[44] The emissions of NO_x from aircraft are for the year 1992 and taken from NASA inventories.[45] Aircraft emissions are implemented in the same manner as lightning emissions so that the total global emission of NO_x from aircraft is 0.85 Tg yr^{-1}.

Three simulations (STOCH-BASE, STOCH-MPN, STOCH-NAPN) were run during this investigation. The STOCH-BASE simulation utilized the CRI v2.2-R5 mechanism[30] and the inclusion of the new loss processes of $CH_3O_2NO_2$ (photolysis and reaction with OH) (Table S2 and S3) where the air parcel contains 240 species competing 805 reactions. The STOCH-MPN simulation was based on the scenario without $CH_3O_2NO_2$ in which the model was run as a 'control' to compare the effects of the addition of $CH_3O_2NO_2$. The other simulation, STOCH-NAPN included the addition of other 44 RO_2NO_2, their formation and degradation reactions. Following the inclusion of RO_2NO_2, the air parcel contains 284 species that compete in 1026 reactions. The comparison of the STOCH-MPN and STOCH-BASE simulations therefore shows the effects of adding the formation and removal of $CH_3O_2NO_2$ on the global composition of the troposphere; and comparison of the STOCH-BASE and STOCH-NAPN simulations shows the effect of the further addition of the formation and removal of the other 44 RO_2NO_2 species.

3. Results and Discussion

3.1. Surface distribution and global burden of RO_2NO_2

The formation of $CH_3O_2NO_2$ is a significant loss pathway for NO_2 in continental regions.[46] Thus the largest mixing ratios of $CH_3O_2NO_2$ up to 10 ppt (Figure 1a) and other 44 RO_2NO_2 up to 4 ppt (Figure 1b) are found at mid-latitudinal land masses corresponding to the areas of the world where there are large-scale industrial activities (e.g. the eastern coast of the USA, central Europe and continental south-east Asia). These regions produce large amounts of NO_x and VOCs, which react in the presence of HO_x to form RO_2NO_2. The zonal plots (Figure 1c and 1d) also showed increased $CH_3O_2NO_2$ with 20-25 ppt and other 44 RO_2NO_2 with 3-6 ppt in the tropics to mid-latitudes of the upper troposphere (9-12 km); which is consistent with the global chemical transport model, GEOS-Chem study (20-35 ppt $CH_3O_2NO_2$ at tropics) by Browne and co-workers.[6] On average, the mixing ratios of $CH_3O_2NO_2$ and other 44 RO_2NO_2 in the upper troposphere are found to be approximately one order of magnitude higher than that found at the surface. For example, in 40-60^{o}N surface, the mixing ratios of other 44 RO_2NO_2 lies between 0.2-0.5 ppt but in the upper troposphere it lies between 2-4 ppt (Figure 1d). This is because the temperatures in the upper troposphere are low enough for other 44 RO_2NO_2 to have increased thermal stability, increasing their lifetimes and mixing ratios.

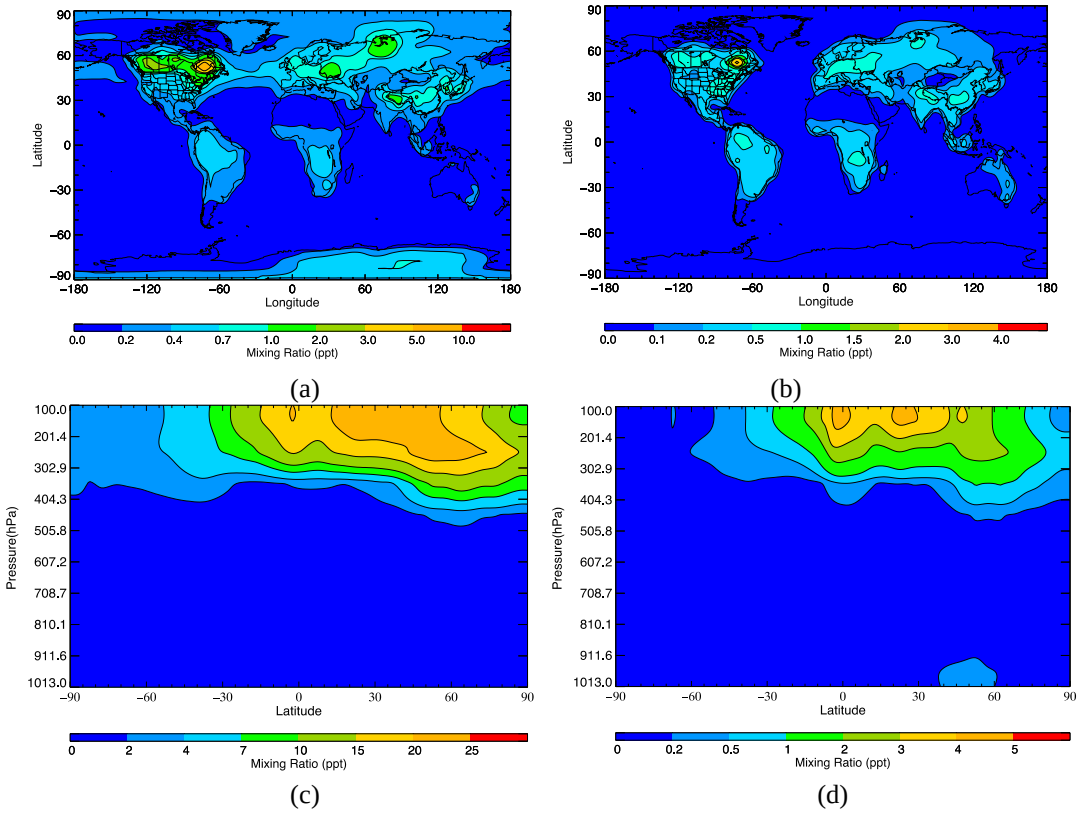

Figure 1. The annual mean mixing ratios of (a) surface $CH_3O_2NO_2$, (b) surface other 44 RO_2NO_2, (c) zonal $CH_3O_2NO_2$, (d) zonal other 44 RO_2NO_2 distribution plots, produced from the STOCHEM-BASE (for $CH_3O_2NO_2$) and STOCH-NAPN (for other 44 RO_2NO_2)

RO_2NO_2 play a large role in the chemistry of the upper troposphere,[6] thus it is important to compare the model vertical profile of RO_2NO_2 with measurement data. The only available measured $CH_3O_2NO_2$ vertical data were obtained during ARCTAS-A (April 2008), DC-3 (June 2012) and SEAC^{4}RS (August-September 2013) campaigns.[14] These were used to compare the modeled data produced by STOCH-NAPN simulation (Figure 2). The modelled data sets for the ARCTAS-A, the DC-3 and the SEAC^{4}RS campaigns show that $CH_3O_2NO_2$ concentrations increase with altitude, which agrees reasonably well with the measurement data. However, in these campaigns, the modelled mixing ratios are underestimated when compared with the measurement data. RO_2NO_2 are very short-lived which makes them extremely difficult for coarse-grid global model, STOCHEM-CRI to accurately predict variations of these species with altitude. The underestimation between modelled and measured values is most apparent in the comparison of the DC-3 and the SEAC^{4}RS campaigns. For ARCTAS-A, the modelled values are within the uncertainty error associated with the measurements, and were only a few ppt outside of this error margin in a few cases (Figure 2a). Whereas for DC-3 and the SEAC^{4}RS, the modelled data are around 10-30 ppt outside of the error associated with the measured data (Figures 2b and 2c). The model-measurement vertical plot of ($CH_3O_2NO_2$+NO_2) shows good agreement throughout the troposphere for ARCTAS-A campaign suggesting that the model is treating the chemistry of $CH_3O_2NO_2$ correctly (Figure S1). However a significant underestimate of the model ($CH_3O_2NO_2$+NO_2) mixing ratios compared with the measured ($CH_3O_2NO_2$+NO_2) mixing ratios for DC-3 and the SEAC^{4}RS campaigns is found in the upper troposphere (Figure S1), although the deviation of the ratio of $CH_3O_2NO_2$/($CH_3O_2NO_2$+NO_2) between model and measurement is not significantly high in the upper troposphere for these two campaigns (Figure S2). The underestimation of the model data compared with the measured data for DC-3 and the SEAC^{4}RS campaigns can be explained by our assumptions concerning underestimated NO_x emissions (lightning). Lightning forms NO_x due to the high temperatures present in the lightning flash, unlike other emissions of NO_x lightning injects these species directly into the troposphere, where they can react with RO_2 to form RO_2NO_2.[47] The STOCHEM model accounts for the emission of NO_x by lightning, with the global emission of 5 Tg yr^{-1}, which falls within the estimated actual emission of global NO_x of 2-8 Tg yr^{-1}.[48] The sampling during the DC-3 and the SEAC^{4}RS campaigns was biased toward fresh convective outflow impacted by lightning NO_x resulting in higher $CH_3O_2NO_2$ formation in the upper troposphere[14] compared with the model $CH_3O_2NO_2$ formation simulated in STOCH-NAPN. The model was run with 1998 meteorology and the emission inventories of RO_2NO_2 precursors e.g. surface anthropogenic VOCs and NO_x from 1998 and aircraft NO_x from 1992 were used in the model whereas the flight

campaigns were from a variety of years, meaning there is likely to be some variation between measured and modelled data.

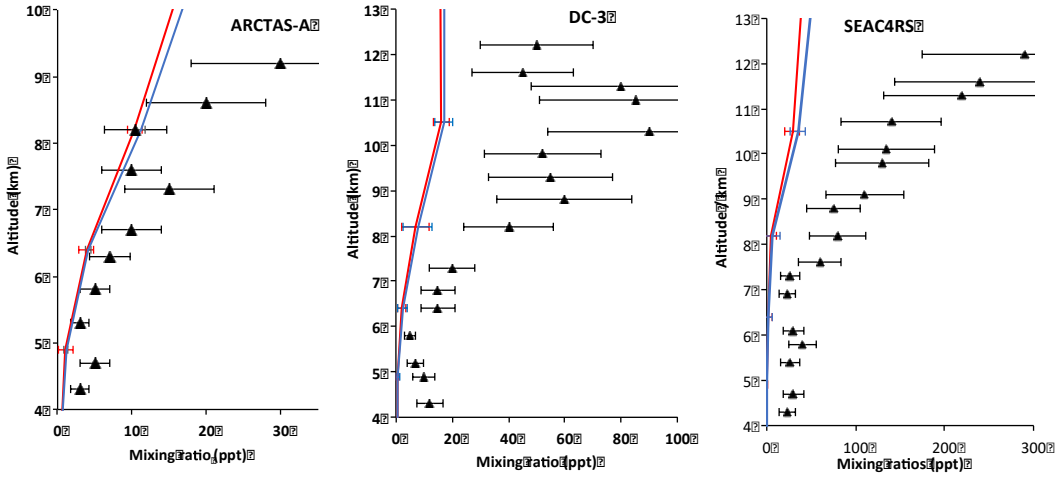

Figure 2 Comparison of measured $CH_3O_2NO_2$ mixing ratios (from (a) the ARCTAS-A and (b) DC-3, (c) SEAC^{4}RS campaigns) with modelled $CH_3O_2NO_2$ and all RO_2NO_2 (including $CH_3O_2NO_2$) mixing ratios. The blue and red lines represent the modelled $CH_3O_2NO_2$ and RO_2NO_2 values, produced by the STOCHEM-BASE and STOCH-NAPN simulation, respectively. The black triangle symbols represent the measurement data collected from Nault et al.[14] The black error bars represent measurement variability. The blue and red error bars represent model errors based on errors in sources and sinks.

The summed mixing ratios of all the RO_2NO_2 (including $CH_3O_2NO_2$) along with $CH_3O_2NO_2$ alone are included in Figure 2 for comparison. The summed RO_2NO_2 mixing ratios are very similar to the sole mixing ratios of $CH_3O_2NO_2$, suggesting that $CH_3O_2NO_2$ makes up a significant proportion of the total amount of RO_2NO_2 present in this simulation. This can be confirmed by the global burden of $CH_3O_2NO_2$ which makes up ~80% of the total global burden of RO_2NO_2 (Table 1).

The summed global burden of all RO_2NO_2 in the STOCH-NAPN simulation amounts to 74.1 Gg. After $CH_3O_2NO_2$, isoprene derived peroxy nitrates and monoterpene derived peroxy nitrates make up the most significant contributions of 3.6 Gg (~5%) and 2.9 Gg (~4%), respectively to the total global burden of RO_2NO_2 (Table 1). The tropospheric lifetimes of the most significant RO_2NO_2 species are also shown in Table 1. The tropospheric lifetimes of isoprene and monoterpenes derived RO_2NO_2 are found to be 6-7 times lower than those of short chain RO_2NO_2 (e.g. $CH_3O_2NO_2$ and $C_2H_5O_2NO_2$), which is mainly due to higher thermal decomposition rates of the large complex RO_2NO_2 (see the individual lifetimes for different loss processes in Supplementary Table S5).

The tropospheric lifetime of $CH_3O_2NO_2$ from the surface to 12 km, has been previously documented[14] and was calculated using observed OH concentrations, photolysis rates and temperatures along with the rate coefficients estimated for the additional loss processes (photolysis and thermal decomposition) of $CH_3O_2NO_2$. The calculated lifetimes by Nault et al.[14] increased linearly with altitude (from 1×10^{-4}

hours to 30 hours). The average tropospheric lifetime of $CH_3O_2NO_2$ obtained from the STOCH-NAPN simulation is 373 s (1.04×10^{-1} hours), which is similar to the calculated lifetime at around 6 km from the study of Nault et al.[14]

Table 1. The lifetimes and global burdens of significant RO_2NO_2 in the STOCH-NAPN simulation. The percent contributions to the total RO_2NO_2 burden are shown in the parentheses.

RO_2NO_2	**Global burden (Gg)**	**Lifetime (s)**
$CH_3O_2NO_2$	59.6 (80.5)	373
$C_2H_5O_2NO_2$	1.9 (2.6)	542
$HOC_2H_4O_2NO_2$	0.4 (0.5)	200
n-$C_3H_7O_2NO_2$ and i-$C_3H_7O_2NO_2$	0.4 (0.5)	340
n-$C_4H_9O_2NO_2$ and sec-$C_4H_9O_2NO_2$	2.2 (3.0)	336
Isoprene derived peroxy nitrates	3.6 (4.9)	205 ± 190*
Monoterpenes derived peroxy nitrates	2.9 (3.9)	121 ± 53*
Other peroxy nitrates (≥C_3 compounds)	3.1 (4.1)	183 ± 99*
*represents averaged values over all non-acyl peroxy nitrates of this type		

3.2. Impact of RO_2NO_2 chemistry on NO_x

Following the addition of $CH_3O_2NO_2$ into STOCH-MPN and addition of 44 other RO_2NO_2 into STOCH-BASE, NO_x mixing ratios decreased by up to 10% and 5%, respectively over the east coast of the USA, Europe, continental south-east China, where RO_2NO_2 has acted as a sink of NO_2. However, the inclusion of $CH_3O_2NO_2$ chemistry in STOCH-BASE compared with STOCH-MPN has an impact on surface-level NO_x with the increases by up to 70% in north-west Brazil, west of Malaysia, and north of Papa New Guinea case (Figures 3a). The increase in NO_x mixing ratios from the addition of the other 44 RO_2NO_2 chemicals has the same effect i.e., an increase of up to 70% in almost the same regions (Figure 3c). All these regions are relatively remote, tropical locations, which tend to have low background NO_x.[49] This shows the behavior of RO_2NO_2 as a temporary reservoir species, transporting NO_x to remote locate locations from NO_x source regions. Therefore, the increase of NO_x (global burden increase of NO_x by 3.0% in STOCH-BASE compared with STOCH-MPN and by 4.4% in STOCH-NAPN compared with STOCH-BASE) means that when the RO_2NO_2 degrade, the increase in NO_x is relatively large compared with the regions with higher mixing ratios of background NO_x. These increases over remote tropical locations can be seen in the zonal distribution plots up to 25% increase of NO_x at the upper level in the equatorial region (Figure 3b and 3d). The increased levels of NO_x formed at the equator are being carried up into the upper troposphere by convection. In addition, the highest mixing ratios of $CH_3O_2NO_2$ (see Figure 1b) and their dominant loss processes via photolysis in the upper troposphere[50] result in increased amounts of NO_x (up to 10%) produced in the STOCH-BASE case compared with the STOCH-MPN case (Figure 3b). The mixing ratios of 44 other RO_2NO_2 are 4 to 5-fold lower than the mixing ratios of $CH_3O_2NO_2$ (Figure 1), but their losses have become increasingly important in the upper troposphere (see Table S5) making 44 other RO_2NO_2 a significant contributor towards the percentage increase of NO_x by up to 10% (Figure 3d). Despite the high mixing ratios of

$CH_3O_2NO_2$ and 44 other RO_2NO_2 compounds at 30°S-90°N in the upper troposphere (see Figure 1c and 1d), the large increases in NO_x only occur between 30°S and 30°N. The enhanced photolysis rates and increased OH concentrations in the tropics accelerate the degradation of 44 other RO_2NO_2 by photolysis and reaction with OH to enhance NO_x production.

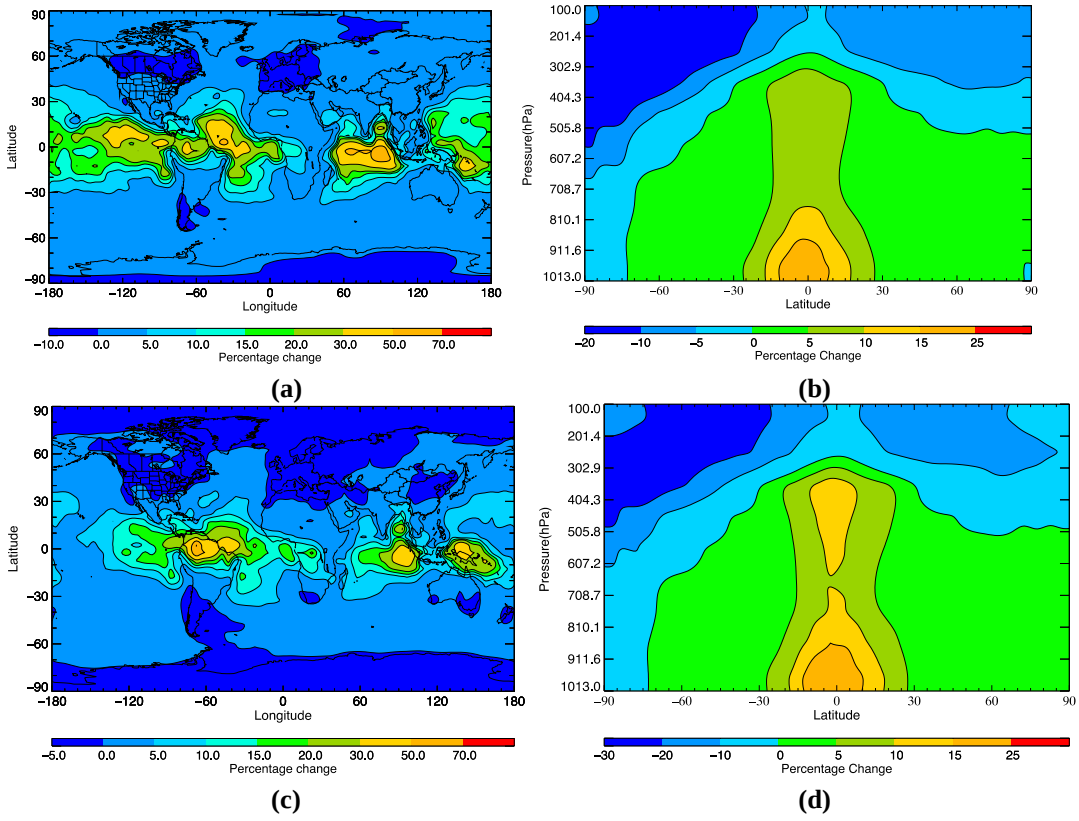

Figure 3. The (a) surface and (b) zonal distribution plots of the percentage change in the annual mean mixing ratios of NO_x between the STOCH-MPN run and STOCH-BASE run, the (c) surface and (d) zonal distribution plots of the percentage change in the annual mean mixing ratios of NO_x between the STOCH-BASE run and STOCH-NAPN run.

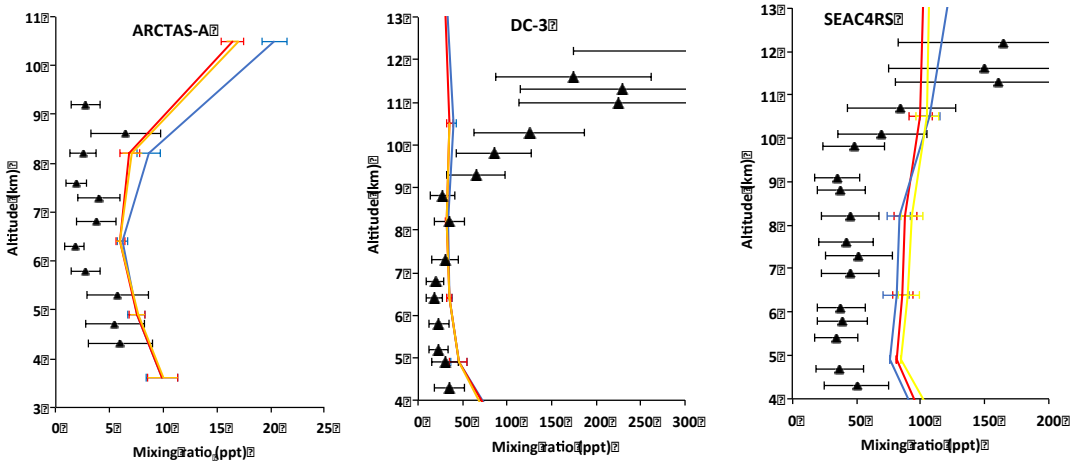

Figure 4 Comparison of measured NO_2 mixing ratios (from (a) the ARCTAS-A, (b) the DC-3 and (c) SEAC^{4}RS campaigns), with modelled mixing ratios. The blue, yellow and red lines represent the model values produced by STOCH-MPN, STOCH-BASE and STOCH-NAPN cases, respectively. The black triangle symbols represent the measurement data collected from Nault et al.[14] Black error bars represent measurement variability. The blue, yellow and red error bars represent model errors based on errors in sources and sinks.

The vertical NO_2 measurement data from ARCTAS-A, DC-3 and SEAC^{4}RS campaigns were compared with modelled mixing ratios of NO_2 simulated by the STOCH-MPN, the STOCH-BASE and the STOCH-NAPN runs. Data from the ARCTAS-A campaign are comparable with the modelled data with several data points falling within the margin of error in the measurement data (see Figure 4a). As well as the general data patterns being very similar: decreasing mixing ratios as altitude increases, up to 7 km, where the mixing ratio starts to increase with altitude. In the DC-3 and SEAC^{4}RS campaigns, the modelled data are comparable with the measured data below 9 km (Figure 4b and 4c). Above this altitude the deviation between the measured and the modelled mixing ratios of NO_2 become larger, which could be explained by the influence of lightning NO_x emissions made by the median air masses for the entire DC-3 and SEAC^{4}RS campaigns more dominated by NO_2.

3.3. Impact of increased NO_x from RO_2NO_2 chemistry on the oxidant levels

The increased production of NO_2 in the tropics due to the addition of the formation and removal chemistry of $CH_3O_2NO_2$ enhanced the production flux of ozone by 2.6% resulting in an increased global burden of ozone by 2.0%, but the addition of the other 44 RO_2NO_2 increased the production flux of ozone by 9.2% causing an increase of ozone global burden by 3.4%. This is supported by the distribution plot of ozone (Figure 5) when compared with the distribution plot of NO_x (Figure 3). The maximum increases in surface tropospheric ozone by up to 16% for inclusion of $CH_3O_2NO_2$ and up to 30% for inclusion of the other 44 RO_2NO_2 occur in the same regions of the maximum increases of NO_x over Brazil, Malaysia, and Papa New Guinea (Figure 5a and 5c). The maximum increases of ozone by up to 8% and 14% due to additions of $CH_3O_2NO_2$ and other 44 RO_2NO_2, respectively were found throughout the troposphere over the equator due to relatively high levels of NO_x produced from the sink processes of $CH_3O_2NO_2$ and other 44 RO_2NO_2 (Figure 5b).

The measured ozone mixing ratios from several different flight campaigns compiled in Emmons et al.[51] and SEAC^{4}RS campaign[52] were compared with modelled ozone mixing ratios simulated by STOCH-BASE, STOCH-MPN and STOCH-NAPN in Figure 6. Due to the increased ozone formation in STOCH-NAPN, the slight improvement between STOCH-BASE and measured ozone mixing ratios are found for all of the flight campaigns. In the TRACE-A and SEAC^{4}RS campaigns there was a high frequency of biomass burning and convective transport, which a global model is not capable of accounting for specifically. This could explain the large difference between the measured and modelled values above Brazil, the South Atlantic and South Africa in the upper troposphere.[53] However, the inclusion of 44

other RO_2NO_2 in the STOCH-NAPN reproduced measured ozone from TRACE-A and SEAC^{4}RS campaigns more accurately than the STOCH-BASE and STOCH-MPN simulations indicating that the addition of 44 other RO_2NO_2 has improved the accuracy of the modelled ozone mixing ratios.

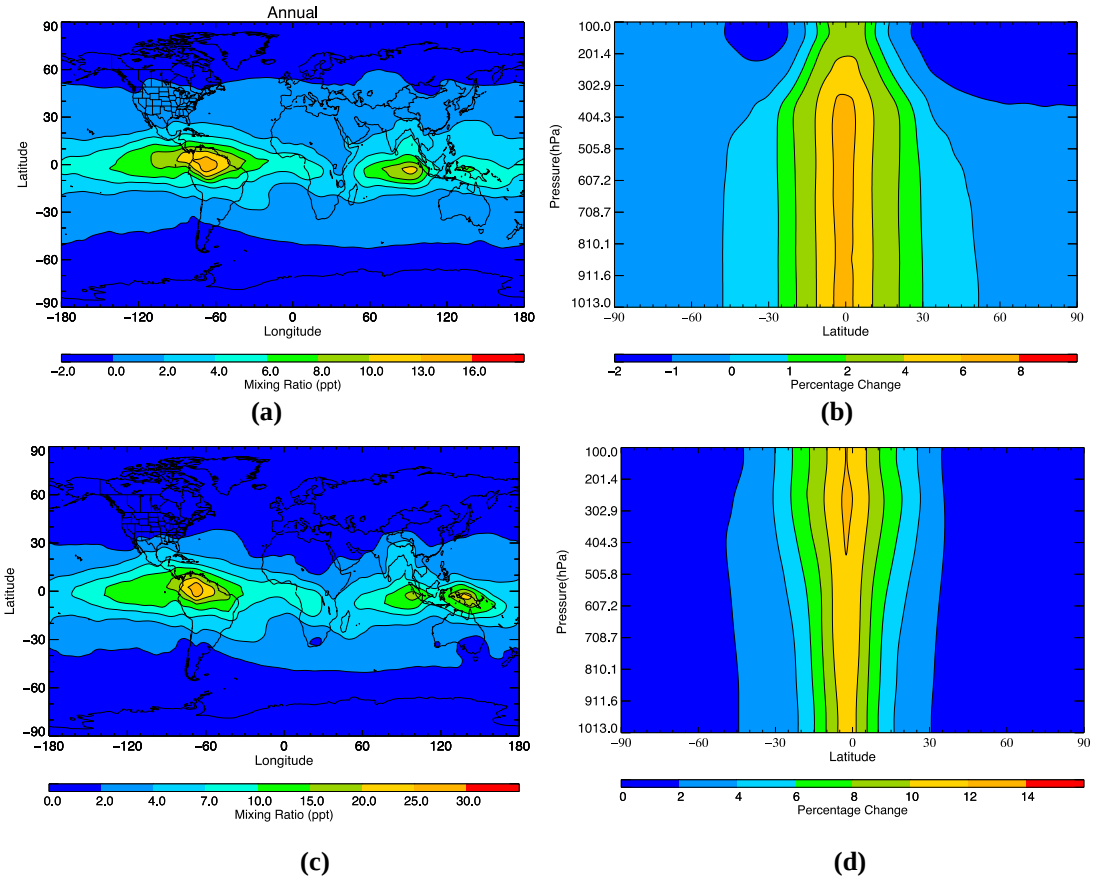

Figure 5. The (a) surface and (b) zonal distribution plots of the percentage change in the annual mean mixing ratios of ozone between the STOCH-MPN run and STOCH-BASE run, the (c) surface and (d) zonal distribution plots of the percentage change in the annual mean mixing ratios of ozone between the STOCH-BASE run and STOCH-NAPN run.

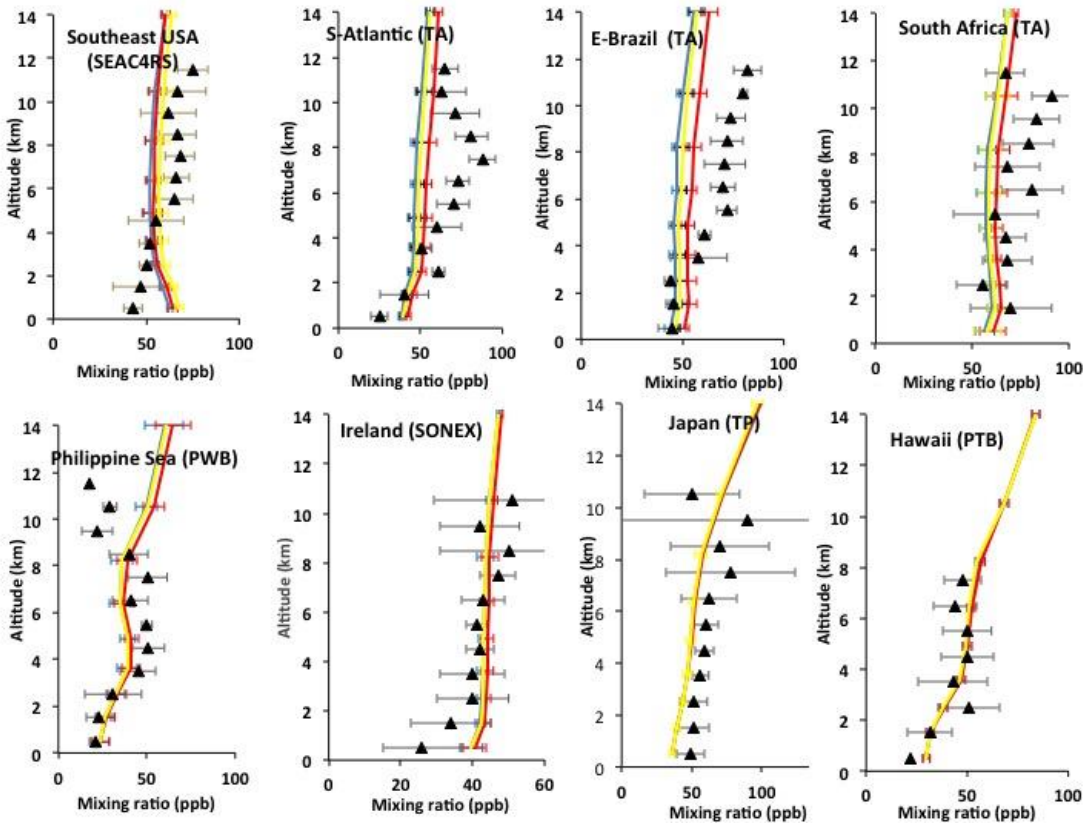

Figure 6 Comparison of measured ozone mixing ratios (black triangles) collected from Emmons et al.[51] and SEAC[4]RS campaign[52] with modelled mixing ratios for both STOCH-BASE (blue line), STOCH-MPN (yellow line) and STOCH-NAPN (red line) simulations. Black error bars represent measurement variability. The blue, yellow and red error bars represent model errors based on errors in sources and sinks

The increased ozone in STOCH-BASE and STOCH-NAPN due to addition of $CH_3O_2NO_2$ and 44 other RO_2NO_2 resulted in increasing the fluxes of the photolysis of ozone, thereby increasing the global burden of $O(^1D)$ by 2.8% and 4.8%, respectively. The reaction of $O(^1D)$ radicals with water accounts for ~46% of the total source of tropospheric OH radicals and the flux of this reaction has increased by 6.7% in STOCH-BASE and 10.5% in STOCH-NAPN compared with STOCH-MPN and STOCH-BASE, respectively. In addition, ~30% and ~9% of the total source of tropospheric OH radicals come from the reaction of HO_2+NO and HO_2+O_3, respectively. The increased NO and O_3 burden due to the addition of $CH_3O_2NO_2$ in the STOCH-BASE and the addition of 44 other RO_2NO_2 in the STOCH-NAPN resulted in increasing the formation flux of OH through the reaction with HO_2 by 6.8% and 7.2% (STOCH-BASE compared with STOCH-MPN) and by 12.7% and 13.5% (STOCH-NAPN compared with STOCH-BASE), respectively. The increased formation fluxes of OH from these three dominant reactions lead to an increase in the global burden of tropospheric OH radicals by 4.0% in STOCH-BASE and 5.5% in STOCH-NAPN, compared with STOCH-MPN and STOCH-BASE, respectively. Figure 7 supports the case that the increase in mixing ratios of the OH radicals occurs in the same regions as the increase in mixing ratios of both ozone and NO_x. Relatively large increases of OH radicals occur over the equator from the surface by up to 30%

(Figure 7a) and 40% (Figure 7c), to the upper troposphere by up to 10% (Figure 7b) and 20% (Figure 7d) due to addition of $CH_3O_2NO_2$ and 44 other RO_2NO_2, respectively.

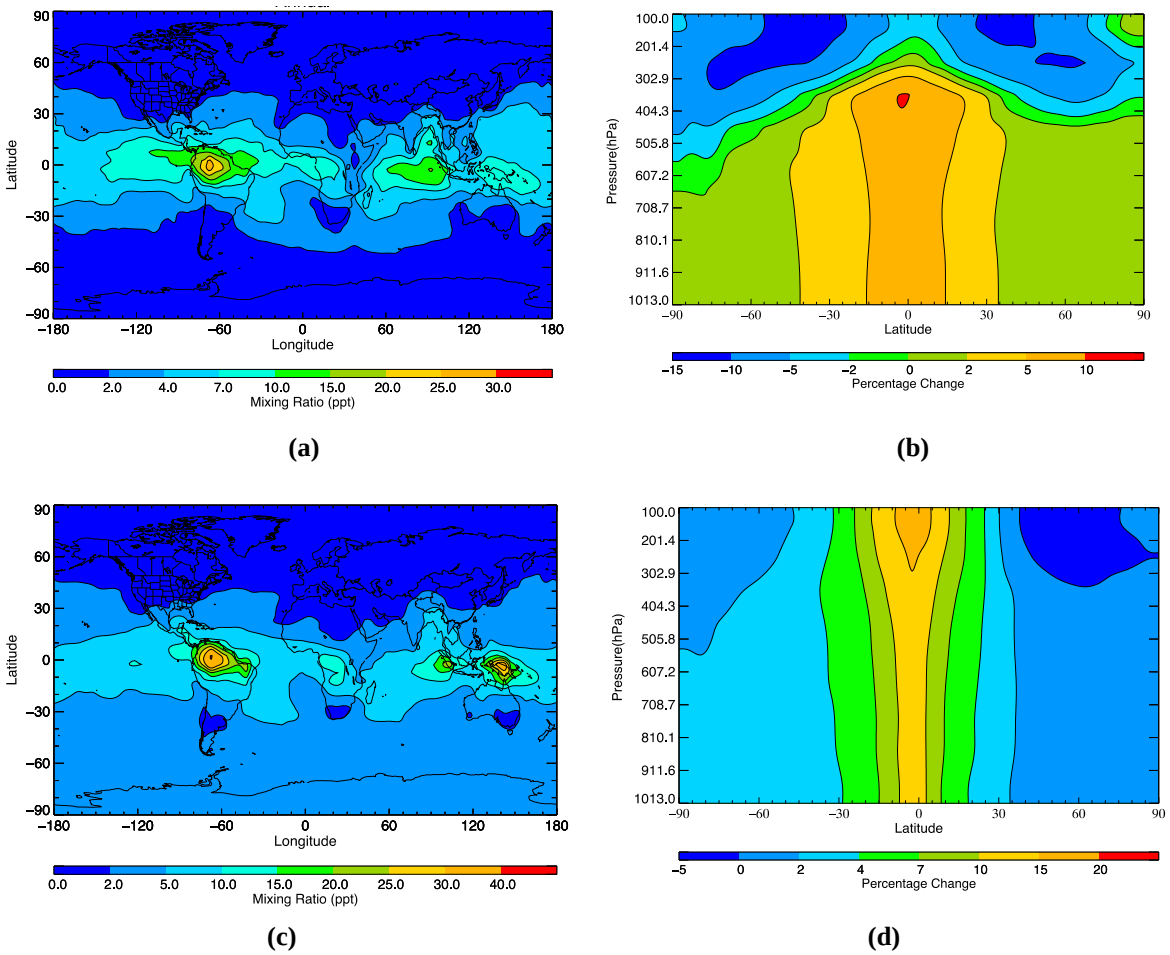

Figure 7. The (a) surface and (b) zonal distribution plots of the percentage change in the annual mean mixing ratios of OH between the STOCH-MPN run and STOCH-BASE run, the (c) surface and (d) zonal distribution plots of the percentage change in the annual mean mixing ratios of OH between the STOCH-BASE run and STOCH-NAPN run.

The increased global burden of OH radicals has implications for the lifetime of many VOCs in the troposphere as OH radicals act as the major sink for most VOCs. Due to the addition of $CH_3O_2NO_2$ and RO_2NO_2 chemistry, the lifetime of CH_4 has decreased by 0.32 year (~5% from STOCH-MPN) and 0.38 year (~6% from STOCH-BASE), respectively. This is a substantial decrease in the calculated lifetime of methane and can have implications for the climate simulations. Methane is an important greenhouse gas, which since the start of the industrial revolution, has been calculated to be responsible for 20% of the warming of the Earth's atmosphere caused by long-lived greenhouse gases.[54] A decrease in the lifetime of methane reduces the capability of this species to warm the Earth's atmosphere.

The nitrate radical, NO_3, is mostly formed from the reaction of NO_2 with ozone in the troposphere. It would follow that the flux of this reaction has increased

by 9.1% in STOCH-BASE and 15.8% in STOCH-NAPN because the addition of $CH_3O_2NO_2$ and 44 other RO_2NO_2 has resulted in increased burdens of both NO_2 and ozone. This resulted in increasing the global burden of NO_3 by 8.8% between the STOCH-BASE and STOCH-NAPN runs and 11.1% between the STOCH-MAPN and STOCH-BASE. The maximum increases of surface NO_3 occurs in the same locations as the maximum increase of surface NO_x, O_3 and OH (see Figure 8a and 8c). This is expected from the flux and global burden data as most of the total source flux of NO_3 comes from reactions involving these species. In the zonal plot of STOCH-BASE (see Figure 8b) where the maximum increase in NO_3 throughout the troposphere occurs over the equator in the upper troposphere. Although, it should be noted that the maximum increases in the mixing ratios of NO_3 are much larger than the maximum increases of the precursor compounds in the same regions. This could be because background levels of NO_3 are very low since STOCHEM distributions are a monthly average, and NO_3 is rapidly photolysed during the day. This means that daytime mixing ratios of NO_3 are very low.

The degradation of $CH_3O_2NO_2$ via photolysis is responsible for ~87% of the flux of NO_3 produced by the photolysis of all non-acyl peroxy nitrates which is ~2% of the total global tropospheric NO_3 production. This results in significant increases in the mixing ratios of NO_3 in the upper troposphere (30°S to 30°N) latitude by up to 1200% (Figure 8b). However the degradation of RO_2NO_2 via reaction by OH is significant for 44 other RO_2NO_2 compared with $CH_3O_2NO_2$ which contribute ~1% of the total global production flux of NO_3. In addition, the increased mixing ratios of NO_2 and ozone due to the addition of 44 other RO_2NO_2 have a significant effect to increase the mixing ratios of NO_3 throughout the upper troposphere (Figure 8d). Higher mixing ratios of NO_3 at the equator and throughout the upper troposphere will lead to increased oxidation of VOCs in these regions. Although, this will only affect the night-time oxidation cycles as NO_3 is rapidly photolysed during the day.

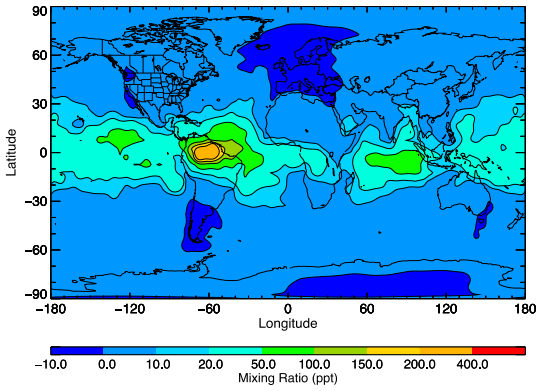

(a)

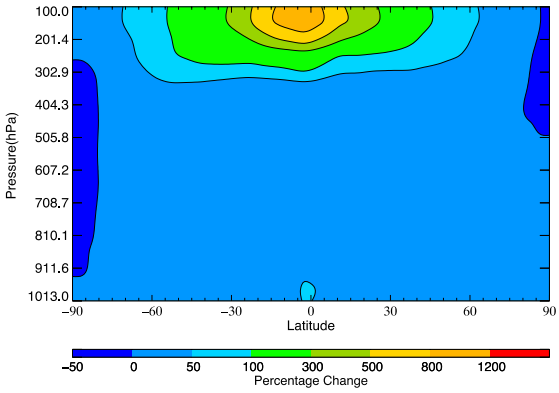

(b)

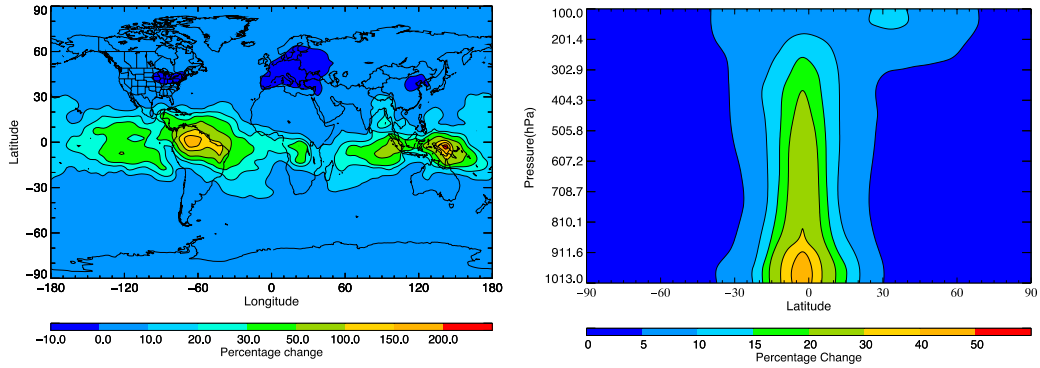

(c) **(d)**

Figure 8 The (a) surface and (b) zonal distribution plots of the percentage change in the annual mean mixing ratios of NO_3 between the STOCH-MPN run and STOCH-BASE run, the (c) surface and (d) zonal distribution plots of the percentage change in the annual mean mixing ratios of NO_3 between the STOCH-BASE run and STOCH-NAPN run.

4. Conclusions

The aim of this investigation was to determine how the addition of the formation and removal of $CH_3O_2NO_2$ and 44 other RO_2NO_2 into the STOCHEM-CRI chemistry transport model would impact the NO_x budget in the upper troposphere. The incorporation of the $CH_3O_2NO_2$ and 44 other RO_2NO_2 led to respective increases in the global NO_x burden of 3.0% and 4.4% and respective increases in NO_x mixing ratios of up to 25% and 25% throughout the troposphere. Because of the coupling of the NO_x and HO_x cycles, the increased NO_x burden has a knock-on effect on the budgets of HO_x, O_3, NO_3 and VOCs present in the troposphere. The formation of O_3, OH and NO_3 have all increased (ozone up to 14%, OH up to 20% and NO_3 up to 30%) in the upper troposphere as a result of including the formation and removal of the 44 other RO_2NO_2 species. As OH and NO_3 are major oxidants in the troposphere, the increase in their budget in the upper troposphere has implications for the lifetimes of VOCs present in the troposphere and it was shown that the average tropospheric lifetime of a potent greenhouse gas, CH_4 was calculated to decrease by ~6%.

The thermal instability of RO_2NO_2 species not only makes them a difficult species to investigate in the laboratory, but also to measure in the troposphere. There has only been one previous case of measured values of a RO_2NO_2 species being taken from the troposphere which was $CH_3O_2NO_2$.[14] Comparing the model data with the limited measured data gave reasonable agreement. The measurements of $CH_3O_2NO_2$ and other RO_2NO_2 would be of particular importance, as these species are found to make a significant impact on the NO_x budget of the upper troposphere.

Supporting Information

The Supporting Information is available free of charge on the ACS Publications website at

Rate coefficients for the formation and loss processes of non-acyl peroxy nitrates (RO_2NO_2) used in the model; Emission inventory of RO_2NO_2 precursors used in the model; The calculated atmospheric life-times of RO_2NO_2 in terms of different loss processes; The model-measurement comparison of $CH_3O_2NO_2+NO_2$ and $CH_3O_2NO_2/((CH_3O_2NO_2+NO_2)$ for different flight campaigns.

Acknowledgement

DES and MAHK thank NERC (grant code-NE/K004905/1), Bristol ChemLabS and the Primary Science Teaching Trust under whose auspices various aspects of this work was supported. CJP work was carried out at Jet Propulsion Laboratory, California Institute of Technology, under contract with the National Aeronautics and Space Administration (NASA), and was supported by the Upper Atmosphere Research and Tropospheric Chemistry Programs.

References

(1) Calvert, J. G.; Mellouki, A.; Orlando, J. J.; Pilling, M. J. The mechanisms of atmospheric oxidation of the oxygenates. Oxford University Press, New York, 2011.

(2) Mills, G. P.; Sturges, W. T.; Salmon, R. A.; Bauguitte, S. J. -B.; Read, K. A.; Bandy, B. J. Seasonal variation of peroxyacetylnitrate (PAN) in coastal Antacrtica measured with a new instrument for the detection of sub-part per trillion mixing ratios of PAN. *Atmos. Chem. Phys.* **2007**, *7*, 4589-4599.

(3) Singh, H. B.; Hanst, P. L. Peroxyacetyl nitrate (PAN) in the unpolluted atmosphere: An important reservoir for nitrogen oxides. *Geophys. Res. Lett.* **1981**, *8*, 941-944.

(4) Hudman, R. C.; Jacob, D. J.; Cooper, O. R.; Evans, M. J.; Heald, C. L.; Park, R. J.; Fehsenfeld, F.; Flocke, F.; Holloway, J.; Hübler, G.; Kita, K.; Koike, M.; Kondo, Y.; Neuman, A.; Nowak, J.; Oltmans, S.; Parrish, D.; Roberts, J. M.; Ryerson, T. Ozone production in transpacific Asian pollution plumes and implications for ozone air quality in California. *J. Geophys. Res.* **2004**, *109*, D23S10 (1-14).

(5) Fischer, E. V.; Jaffe, D. A.; Weatherhead, E. C. Free tropospheric peroxyacetyl nitrate (PAN) and ozone at Mount Bachelor: causes of variability and timescale for trend detection. *Atmos. Chem. Phys.* **2011**, *11*, 5641-5654.

(6) Browne, E. C.; Perring, A. E.; Wooldridge, P. J.; Apel, E.; Hall, S. R.; Huey, L. G.; Mao, J.; Spencer, K. M.; Clair, J. M. St.; Weinheimer, A. J.; Wisthaler, A.; Cohen, R. C. Global and regional effects of the photochemistry of $CH_3O_2NO_2$: evidence from ARCTAS. *Atmos. Chem. Phys.* **2011**, *11*, 4209-4219.

(7) Khan, M. A. H.; Cooke, M. C.; Utembe, S. R.; Archibald, A. T.; Derwent, R. G.; Jenkin, M. E.; Leather, K. E.; Percival, C. J.; Shallcross, D. E. Global budget and distribution of peroxyacetyl nitrates (PAN) for present and preindustrial scenarios. *Int. J. Earth Environ. Sci.* **2017**, *2*, 130 (1-10).

(8) Orlando, J. J.; Tyndall, G. S. Laboratory studies of organic peroxy radical chemistry: an overview with emphasis on recent issues of atmospheric significance. *Chem. Soc. Rev.* **2012**, *41*, 6294-6317.

(9) Jenkin, M. E.; Valorso, R.; Aumont, B.; Rickard, A. R. Estimation of rate coefficients and branching ratios for reactions of organic peroxy radicals for use in automated mechanism construction. *Atmos. Chem. Phys.* **2019**, *19*, 7691-7717.

(10) Murphy, J. H.; Thornton, J. A.; Wooldridge, P. J.; Day, D. A.; Rosen, R. S.; Cantrell, C.; Shetter, R. E.; Lefer, B.; Cohen, R. C. Measurements of the sum of HO_2NO_2 and $CH_3O_2NO_2$ in the remote troposphere. *Atmos. Chem. Phys.* **2004**, *4*, 377-384.

(11) Stevens, E. R. The formation, reactions, and properties of peroxyacetyl nitrates (PANs) in photochemical air pollution. *Adv. Environ. Sci. Technol.* **1969**, *1*, 119-147.

(12) Roberts, J. M. PAN and related compounds, in: Volatile Organic Compounds in the Atmosphere, Koppmann, R. (Ed.), Blackwell, Ames, Iowa, USA, 221-268, 2007.

(13) Kim, S.; Huey, L. G.; Stickel, R. E.; Tanner, D. J.; Crawford, J. H.; Olson, J. R.; Chen, G.; Brune, W. H.; Ren, X.; Lesher, R.; Wooldridge, P. J.; Bertram, T. H.; Perring, A.; Cohen, R. C.; Lefer, B. L.; Shetter, R. E.; Avery, M.; Diskin, G.; Sokolik, I. Measurement of HO_2NO_2 in the free troposphere during the Intercontinental Chemical Transport Experiment-North America 2004. *J. Geophys. Res.* **2007**, *112*, D12S01 (1-10).

(14) Nault, B. A.; Garland, C.; Pusede, S. E.; Wooldridge, P. J.; Ullmann, K.; Hall, S. R.; Cohen, R. C. Measurements of $CH_3O_2NO_2$ in the upper troposphere. *Atmos. Meas. Tech.* **2015**, *8*, 987-997.

(15) Roberts, J. M. The atmospheric chemistry of organic nitrates. *Atmos. Environ.* **1990**, *24A*, 243-287.

(16) Lightfoot, P. D.; Cox, R. A.; Crowley, J. N.; Destriau, M.; Hayman, G. D.; Jenkin, M. E.; Moortgat, G. K.; Zabel, F. Organic peroxy radicals: kinetics, spectroscopy and tropospheric chemistry. *Atmos. Environ.* **1992**, *26A*, 1805-1964.

(17) Zabel, F.; Reimer, A.; Becker, K. H.; Fink, E. H. Thermal decomposition of alkyl peroxynitrates. *J. Phys. Chem.* **1989**, *93*, 5500-5507.

(18) Nault, B. A.; Laughner, J. L.; Wooldridge, P. J.; Crounse, J. D.; Dibb, J.; Diskin, G.; Peischl, J.; Podolske, J. R.; Pollack, I. B.; Ryerson, T. B.; Scheuer, E.; Wennberg, P. O.; Cohen, R. C. Lightning NO_x emissions: Reconciling measured and modeled estimates with updated NO_x chemistry. *Geophys. Res. Lett.* **2016**, *44*, 9479-9488.

(19) Thompson, A. M.; Singh, H. B.; Stewart, R. W.; Kucsera, T. L.; Kondo, Y. A Monte Carlo study of upper tropospheric reactive nitrogen during the Pacific Exploratory Mission in the Western Pacific Ocean (PEN-West B). *J. Geophys. Res.* **1997**, *102*, 28437-28446.

(20) Cantrell, C. A.; Mauldin, L.; Zondlo, M.; Eisele, F.; Kosciuch, E.; Shetter, R.; Lefer, B.; Hall, S.; Campos, T.; Ridley, B.; Walega, J.; Fried, A.; Wert, B.; Flocke, F.; Weinheimer, A.; Hannigan, J.; Coffey, M.; Atlas, E.; Stephen, S.; Heikes, B.; Snow, J.; Blake, D.; Blake, N.; Katzenstein, A.; Lopez, J.; Browell, E. V.; Dibb, J.; Scheuer, E.; Seid, G.; Talbot, R. Steady state free radical budgets and ozone photochemistry during TOPSE. *J. Geophys. Res.* **2003**, *108*, 8361 (1-22).

(21) Cullen, M. J. The unified forecast/climate model. *Meteorol. Mag.* **1993**, *122*, 81-94.

(22) Collins, W. J.; Stevenson, D. S.; Johnson, C. E.; Derwent, R. G. Tropospheric ozone in a global-scale three-dimensional Lagrangian model and its response to NOx emission controls. *J. Atmos. Chem.* **1997**, *26*, 223-274.

(23) Johns, T. C.; Carnell, R. E.; Crossley, J. F.; Gregory, J. M.; Mitchell, J. F. B.; Senior, C. A.; Tett, S. F. B., Wood, R. A. The second Hadley Centre coupled ocean-atmosphere GCM: model description, spinup and validation. *Clim. Dyn.* **1997**, *13*, 103-134.

(24) Stevenson, D. S.; Collins, W. J.; Johnson, C. E.; Derwent, R. G. Intercomparison and evaluation of atmospheric transport in a Lagrangian model (STOCHEM), and an Eulerian model (UM), using ^{222}Rn as a short-lived tracer. *Quart. J. Royal Meteorol. Soc.* **1998**, *124*, 2477-2492.

(25) Derwent, R. G.; Stevenson, D. S.; Doherty, R. M.; Collins, W. J.; Sanderson, M. G. How is surface ozone in Europe linked to Asian and North American NO_x emissions? *Atmos. Environ.* **2008**, *42*, 7412-7422.

(26) Collins, W. J.; Stevenson, D. S.; Johnson, C. E.; Derwent, R. G. The role of convection in determining the budget of odd hydrogen in the upper troposphere. *J. Geophys. Res.* **1999**, *104*, 26927-26941.

(27) Jenkin, M. E.; Watson, L. A.; Utembe, S. R.; Shallcross, D. E. A Common Representative Intermediates (CRI) mechanism for VOC degradation. Part 1: Gas phase mechanism development. *Atmos. Environ.* **2008**, *42*, 7185-7195.

(28) Watson, L. A.; Shallcross, D. E.; Utembe, S. R.; Jenkin, M. E. A Common Representative Intermediate (CRI) mechanism for VOC degradation. Part 2: gas phase mechanism reduction. *Atmos. Environ.* **2008**, *42*, 7196-7204.

(29) Utembe, S. R.; Watson, L. A.; Shallcross, D. E.; Jenkin, M. E. A Common Representative Intermediates (CRI) mechanism for VOC degradation. *Atmos. Environ.* **2009**, *43*, 1982-1990.

(30) Jenkin, M. E.; Khan, M. A. H.; Shallcross, D. E.; Bergström, R.; Simpson, D.; Murphy, K. L. C.; Rickard, A. R. The CRI v2.2 reduced degradation scheme for isoprene. *Atmos. Environ.* **2019**, *212*, 172-182.

(31) Jenkin, M. E., Valorso, R., Aumont, B., Rickard, A. R., and Wallington, T. J.: Estimation of rate coefficients and branching ratios for gas-phase reactions of OH with aliphatic organic compounds for use in automated mechanism construction, *Atmos. Chem. Phys.* **2018**, *18*, 9297–9328.

(32) DeMore, W. B.; Golden, D. M.; Hampson, R. F.; Howard, C. J.; Kurylo, M. J.; Molina, M. J.; Ravishankara, A. R.; Sander, S. P. Chemical kinetics and photochemical data for use in stratospheric modeling, Evaluation number 10. JPL Publication 92-20, Jet Propulsion Laboratory, California Institute of Technology, Pasadena, CA, 1992.

(33) Sander, S. P.; Golden, D. M.; Kurylo, M. J.; Moortgat, G. K.; Wine, P. H.; Ravishankara, A. R.; Kolb, C. E.; Molina, M. J.; Finlayson-Pitts, B. J.; Huie, R. E., Orkin, V. L. Chemical kinetics and photochemical data for use in Atmospheric Studies: Evaluation Number 15. Technical report, NASA JPL Publications 06-2, 2006.

(34) Olivier, J. G.; Bouwman, A. F.; Berdowski, J. J.; Veldt, C.; Bloos, J. P.; Visschedijk, A. J.; Zandveld, P. Y.; Haverlag, J. L. A set of global emission inventories of greenhouse gases and ozone-depleting substances for all

anthropogenic and most natural sources on a per country basis and on 1 degree × 1 degree grid. Technical Report, Netherlands Environmental Assessment Agency, 1996.

(35) Collins, W. J.; Stevenson, D. S.; Johnson, C. E.; Derwent, R. G. The European regional ozone distribution and its links with the global scale for the years 1992 and 2015. *Atmos. Environ.* **2000**, *34*, 255-267.

(36) Granier, C.; Lamarque, J. F.; Mieville, A.; Muller, J. F.; Olivier, J.; Orlando, J.; Peters, J.; Petron, G.; Tyndall, S.; Wallens, S. POET, a database of surface emissions of ozone precursors. Retrieved from http://accent.aero.jussieu.fr/database_table_inventories.php (last accessed on 07 April 2020)

(37) Mikaloff-Fletcher, S. E.; Tans, P. P.; Bruhwiler, L. M.; Miller, J. B.; Heimann, M. CH_4 sources estimated from atmospheric observations of CH_4 and its $^{13}C/^{12}C$ isotopic ratios: 1. Inverse modeling of source processes. *Glob. Biogeochem. Cycles* **2004**, *18*, GB4004 (1-17).

(38) Houweling, S.; Dentener, F.; Lelieveld, J.; Walter, B.; Dlugokencky, E. The modeling of tropospheric methane- How well can point measurements be reproduced by a global model? *J. Geophys. Res.* **2000**, *105*, 8981-9002.

(39) Henze, D. K.; Seinfeld, J. H.; Ng, N. L.; Kroll, J. H.; Fu, T. M.; Jacob, D. J.; Heald, C. L. Global modeling of secondary organic aerosol formation from aromatic hydrocarbons: high vs. low-yield pathways. *Atmos. Chem. Phys.* **2008**, *8*, 2405-2420.

(40) Li, D.; Shine, K. P. A 4-dimensional ozone climatology for UGAMP models, Internal Rep. 35, Technical Report, University of Reading, 1995.

(41) Murphy, D. M.; Fahey, D. W. An estimate of the flux of stratospheric reactive nitrogen and ozone into the troposphere. *J. Geophys. Res.* **1994**, *99*, 5325-5332.

(42) Price, C.; Rind, D. A simple lightning parameterization for calculating global lightning distributions. *J. Geophys. Res. Atmos.* **1992**, *97*, 9919-9933.

(43) Price, C.; Penner, J.; Prather, M. NO_x from lightning 1. Global distribution based on lightning physics. *J. Geophys. Res.* **1997**, *102*, 5929-5941.

(44) Pickering, K. E.; Wang, Y.; Tao, W. -K.; Price, C.; Müller, J. -F. Vertical distributions of lightning NO_x for use in regional and global chemical transport models. *J. Geophys. Res.* **1998**, *103*, 31203-31216.

(45) Penner, J. E.; Lister, D. H.; Griggs, D. J.; Dokken, D. J.; Mc-Farland, M. IPCC special report on Aviation and the Global Atmosphere. Technical report, The Intergovernmental Panel on Climate Change, 1999.

(46) Liang, J. Y.; Horowitz, L. W.; Jacob, D. J.; Wang, Y. H.; Fiore, A. M.; Logan, J. A.; Gardner, G. M.; Munger, J. W. Seasonal budgets of reactive nitrogen species and ozone over the United States and export fluxes to the global atmosphere. *J. Geophys. Res.* **1998**, *103*, 13435-13450.

(47) Murray, L. Lightning NO_x and impacts on air quality. *Curr. Pollut. Rep.* **2016**, *2*, 115-133.

(48) Schumann, U.; Huntrieser, H. The global lightning-induced nitrogen oxides source. *Atmos. Chem. Phys.* **2007**, *7*, 3823-3907.

(49) Pike, R. C.; Lee, J. D.; Young, P. J.; Carver, G. D.; Yang, X.; Warwick, N.; Moller, S.; Misztal, P.; Langford, B.; Stewart, D.; Reeves, C. E.; Hewitt, C. N.; Pyle, J. A. NO_x and O_3 above a tropical rainforest: an analysis with a global and box model. *Atmos. Chem. Phys.* **2010**, *10*, 10607-10620.

(50) Palmer, P. The Atmosphere: a very short introduction, Oxford University Press, Oxford, 2017.

(51) Emmons, L. K.; Hauglustaine, D. A.; Müller, J. –F.; Carroll, M. A.; Brasseur, G. P.; Brunner, D.; Staehelin, J.; Thouret, V.; Marenco, A. Data composites of airborne observations of tropospheric ozone and its precursors. *J. Geophys. Res. Atmos.* **2000**, *105*, 20497-20538.

(52) Silvern, R. F.; Jacob, D. J.; Travis, K. R.; Sherwen, T.; Evans, M. J.; Cohen, R. C.; Laughner, J. L.; Hall, S. R.; Ullmann, K.; Crounse, J. D.; Wennberg, P. O.; Peischl, J.; Pollack, I. B. Observed NO/NO_2 ratios in the upper troposphere imply errors in NO-NO2-O3 cycling kinetics or an unaccounted NOx reservoir. *Geophys. Res. Lett.* **2018**, *45*, 4466-4474.

(53) Pickering, K. E.; Thompson, A. M.; Wang, Y.; Tao, W. K.; McNamara, D. P.; Kirchhoff, V. W.; Heikes, B. G.; Sachse, G. W.; Bradshaw, J. D.; Gregory, G. L.; Blake, D. R. Convective transport of biomass burning emissions over Brazil during TRACE A. *J. Geophys. Res. Atmos.* **1996**, *101*, 23993-24012.

(54) Kirschke, S.; Bousquet, P.; Ciais, P.; Saunois, M.; Canadell, J. G.; Dlugokencky, E. J.; Bergamaschi, P.; Bergmann, D.; Blake, D. R.; Bruhwiler, L.; Cameron-Smith, P.; Castaldi, S.; Chevallier, F.; Feng, L.; Fraser, A.; Heimann, M.; Hodson, E. L.; Houweling, S.; Josse, B.; Fraser, P. J.; Krummel, P. B.; Lamarque, J. -F.; Langenfelds, R. L.; Le Quéré, C.; Naik, V.; O'Dohery, S.; Palmer, P. I.; Pison, I.; Plummer, D.; Poulter, B.; Prinn, R. G.; Rigby, M.; Ringeval, B.; Santini, M.; Schmidt, M.; Shindell, D. T.; Simpson, I. J.; Spahni, R.; Steele, L. P.; Strode, S. A.; Sudo, K.; Szopa, S.; van der Werf, G. R.; Voulgarakis, A.; van Weele, M.; Weiss, R. F.; Williams, J. E.; Zeng, G. Three decades of global methane sources and sinks. *Nature Geosci.* **2013**, *6*, 813-823.

FOR TOC ONLY

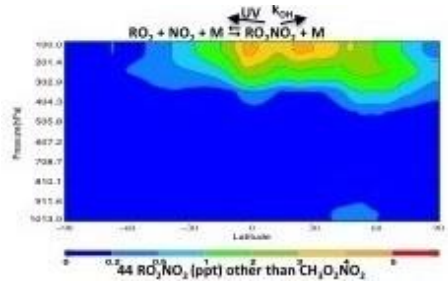
UV
k_{OH}
$RO_2 + NO_2 + M \rightleftharpoons RO_2NO_2 + M$
Latitude
44 RO_2NO_2 (ppt) other than $CH_3O_2NO_2$